

Technology options for imaging spectrometry

A.R. Harvey^{*a}, J. Beale^b, A. H. Greenaway^b, T. J. Hanlon^a, J. Williams^b

^aDepartment of Aerospace, Power and Sensors, Cranfield University, Shrivenham,
Swindon, SN6 8LA, UK

^bDERA, St Andrews Rd., Malvern, Worcestershire, WR14 3PS, UK

ABSTRACT

The principles for defining, comparing and calculating the signal-to-noise ratio performance of imaging spectrometers are presented. The relative signal-to-noise ratios (SNRs) of the main classes of imaging spectrometer are discussed both in general terms and with an emphasis on real-time, low spectral resolution applications. This general analysis is based on some simplifying assumptions and SNRs are also calculated for a typical application without these assumptions. These SNRs are compared to the signal-to-noise ratios typically required in imaging spectrometry. It is shown that for low resolution imaging spectrometry of low radiance scenes there are only small differences in SNR between the four main classes of instrument. For high spectral resolution imaging of low radiance scenes Fourier-transform techniques offer higher SNRs, but for high radiance scenes the impact of detector saturation tends to favor direct imaging spectrometry. It is noted however, that real-time, temporally scanned, imaging spectrometry requires track and stare stabilization to fully realize its potential.

1. INTRODUCTION

In recent years, many approaches to imaging spectrometry have been proposed and demonstrated and of all the aspects that determine the usefulness of a particular technique, perhaps the most significant is the achievable signal-to-noise ratio (SNR). The authors have a specific interest in the application of imaging spectrometry to real-time surveillance, for which a typical update rate for the complete spectral data cube is a few tens of Hz. For wide-angle surveillance the maximum frame rate obtainable from off-the-shelf cameras limits the number of spectral bands to perhaps 20 or so. This spectral resolution is considerably less than is normally considered as hyperspectral imaging and the relative importance of the parameters that determine the SNR are somewhat different. In particular, for a spectrally multiplexed imaging spectrometer, such as is implemented with a rotating filter wheel, the irradiance at the detector is proportionate to $1/N^2$, where N is the number of spectral bands and so when N is small, the detector is far more likely to become saturated than in high-resolution hyperspectral imaging. In this paper, we discuss in fundamental and general terms, the relative signal-to-noise ratios that can be obtained by different types of imaging spectrometer including when the detector saturation occurs. To the knowledge of the authors a general and fundamental comparison of SNRs of imaging spectrometers has not previously been published.

All approaches to imaging spectrometry can be conveniently classified as direct or indirect: either the spectrum is recorded directly with a direct imaging spectrometer (DIS) based on a wavelength selective element such as a prism or bandpass filter, or an indirect method in which an inversion of a measured intensity distribution is required. This latter approach is exemplified by the Fourier-transform imaging spectrometer (FTIS). For each of these classes the required optical intensity distributions are recorded by either temporal scanning as with spectral multiplexing or a conventional Fourier-transform spectrometer or alternatively the data is obtained in a snapshot by spatially dispersing the input light as with a dispersive spectrometer or a spatial Fourier-transform spectrometer. The four classes of instrument are thus the DIS which is subdivided into snapshot or fully-staring DIS (labeled here as FS-DIS) and temporally multiplexed DIS, and the FTIS which is subdivided into temporally scanned FTIS and snapshot (FS-FTIS) varieties. This taxonomy is illustrated in Table 1.

Examples of a DIS include tunable Fabry-Perot filters¹, rocking interference filters, wedge filters², rotating filter wheels and linearly variable and circularly variable filters. The salient disadvantage of these temporally multiplexed DIS is that the temporal multiplexing reduces integration time and SNR compared to a FS-DIS. The classical push-broom scanned (PBS) imaging spectrometer based on spectral dispersion of the image of a slit is the most obvious example of the FS-DIS^{3,4,5,6,7} although approaches based on spectrometry of single photons⁸ and fiber-bundle-coupled spectrographs have also been reported in addition to the conventional color TV camera. The former and latter examples of the FS-DIS illustrate the dilemma of this approach; either high spectral resolution of a small or one-dimensional field of view is possible or low spectral resolution of a wide field of view is easily implemented, but wide field of view and high spectral resolution are not simultaneously readily achievable. A major advantage of the FS-DIS is that coregistration of all spectral sub-images is more straightforward than for the temporally multiplexed DIS. Temporally scanned FTIS instruments are normally based on

* Correspondence: Email: a.r.harvey@rmcs.cranfield.ac.uk,

WWW: http://www.rmcs.cranfield.ac.uk/departments/daps/Groups/Electro_optics/harvey.htm;

Telephone: +44 (0)1793 785215; Fax +44 (0)1793 785902

mechanically scanned interferometers^{9,10} and the FS-FTIS is based on a Sagnac interferometer using an achromatically dispersed image of a slit¹¹ although Wollaston prisms may also be used¹². Some prominent techniques that do not neatly fit into the above taxonomy, such as the computed tomography imaging spectrometer¹³ and the diffractive optic imaging spectrometer¹⁴ do not lend themselves so readily to SNR analysis as the prototype techniques above. However, it is noted that both instruments are essentially transform devices and therefore the conclusions presented here for the FTIS and FS-FTIS are probably the closest approximations. For the technique called HEIFTS¹⁵, SNR expressions for a temporally scanned FTIS should be used, although topologically this instrument is more similar to a FS-FTIS.

In the next section we derive approximate values for the SNR required of imaging spectrometers for spectral classification and in sections 3 and 4 we derive expressions for the SNRs of a DIS and FTIS that enable their comparison in section 5 in both general terms and with simplifying assumptions. The same equations are used in section 6 to compare the SNRs of the one-dimensional push-broom scanned, FS-DIS and FS-FTIS. In section 6 we underline that although the temporally scanned DIS and FTIS enable higher SNRs to be attained than the one-dimensional PBS FS-DIS and FS-FTIS, it will probably only be possible to exploit this advantage in real-time applications if the coregistration problems can be solved by using, for example, step-stare stabilization. Comparison of the SNRs achievable by the four techniques was possible only because some simplifications were made in the analysis and in section 7 we calculate the SNRs for an example application without needing to resort to these simplifications and in section 8 we present conclusions.

	Temporally scanned	Snap shot
Direct	<p>DIS</p>	<p>FS-DIS</p>
Fourier-transform	<p>FTIS</p>	<p>FS-FTIS</p>

Table 1 Depiction of the multiplexing modes for construction of spectral image cubes

2. REQUIRED SIGNAL-TO-NOISE RATIO

In this section we estimate the SNR required at the output of a spectral imager to yield a particular SNR at the output of a matched filter and values are presented based on example spectra¹⁶. This knowledge enables the design of an instrument with an SNR that is necessary and sufficient for a task. The spectral correlation coefficient may be expressed as the covariance between a set of spectral measurements $S_1, S_2, S_3, \dots, S_N$ and a matched filter template $T_1, T_2, T_3, \dots, T_N$ which may be written as

$$r = \frac{\sum_{i=1}^N (T_i - \bar{T})(S_i - \bar{S})}{\sqrt{\sum_{i=1}^N (T_i - \bar{T})^2 \sum_{i=1}^N (S_i - \bar{S})^2}} \quad (1)$$

where \bar{S} and \bar{T} represent mean values of the spectrum and template. In practice the spectrum $S_1 \dots S_N$ is contaminated by a random noise vector $\epsilon_1 \dots \epsilon_N$ which reduces the measured correlation by a value Δr from the true value r . Rewriting equation (1) in vector form and applying a binomial expansion gives

$$r + \Delta r = \frac{\mathbf{T} \cdot (\mathbf{S} + \boldsymbol{\epsilon})}{\sqrt{\mathbf{T} \cdot \mathbf{T} (\mathbf{S} + \boldsymbol{\epsilon}) \cdot (\mathbf{S} + \boldsymbol{\epsilon})}} \Rightarrow \text{SD}(\Delta r) \approx r \text{SD} \left(\frac{\mathbf{T} \cdot \boldsymbol{\epsilon}}{\mathbf{T} \cdot \mathbf{T}} - \frac{\mathbf{S} \cdot \boldsymbol{\epsilon}}{\mathbf{S} \cdot \mathbf{S}} - \frac{\boldsymbol{\epsilon} \cdot \boldsymbol{\epsilon}}{2\mathbf{S} \cdot \mathbf{S}} \right). \quad (2)$$

That is, if we make a set of nominally equivalent measurements of the spectral correlation for different noise vectors $\boldsymbol{\epsilon}$ then we obtain a set of measurements of $r + \Delta r$ which will have a standard deviation equal to the standard deviation in Δr . For high correlations, the first two terms cancel and the last term dominates. The signal-to-noise ratio in the correlation is then

$$\text{SNR}(r)_{\text{HiCorr}} = 2\sqrt{N} \left(\frac{\hat{S}}{S} \text{SNR}(S) \right)^2 \quad (3)$$

where \hat{S} denotes the RMS value of $S_1 \dots S_N$.

When $\hat{S} > \hat{\epsilon}$ and for low values of correlation, $\mathbf{T} \cdot \mathbf{S} < \mathbf{S} \cdot \mathbf{S} < \mathbf{S} \cdot \boldsymbol{\epsilon}$, so the standard deviation on Δr is dominated by the first term. We can therefore write

$$\text{SNR}(r)_{\text{LoCorr}} = \sqrt{N} r \frac{\hat{S}}{S} \text{SNR}(S) \quad (4)$$

and this expression is generally accurate for $r \leq 1/2$. Of course, the SNR varies across the spectrum and so equations (3) and (4) need to be used judiciously. For shot-noise limited spectrometry the signal-to-noise ratio, $\text{SNR}(S)$, tends to decrease with the square root of the number of spectral bands, so the output SNR is independent of N for low correlations, but is inversely proportional to the square root of N for high correlations. For detector-noise limited imaging $\text{SNR}(S)$ is inversely proportional to N and so $\text{SNR}_{\text{LoCorr}}$ is inversely proportional to \sqrt{N} and $\text{SNR}_{\text{HiCorr}}$ is inversely proportional to N . This suggests that N should be the smallest possible value that captures the spectral information present in \mathbf{S} .

Equations (3) and (4) have been applied to the discrimination between similar spectra in the Aster spectral data base¹⁶. For $N \sim 10-20$ and for dissimilar spectra we calculate minimum required signal-to-noise ratios of the order of unity, but for the more pertinent case of discriminating between similar spectra, we estimate required signal-to-noise ratios of several hundred. For imaging in 100 bands SNRs of up to about 100 are desirable.

3. SIGNAL-TO-NOISE RATIO OF DIRECT IMAGING SPECTROMETERS

The signal-to-noise ratio at the output of a DIS can be written as

$$\text{SNR} = \frac{e_s}{\sqrt{\bar{n}_d^2 + \bar{e}_s + \bar{e}_b}} \quad (5)$$

Where e_s is the number of signal photoelectrons measured during the integration time, \bar{n}_d is the RMS number of noise electrons associated with reading the detector, \bar{e}_s is the RMS photon shot noise on the recorded signal flux and \bar{e}_b is the RMS photon shot noise on the background flux. We can substitute the following quantities into (5)

$$e_s = \bar{e}_s = T \int_{\lambda}^{\lambda+d\lambda} k_s(\lambda) d\lambda \quad \bar{e}_b = T \int_{\lambda}^{\lambda+d\lambda} k_b(\lambda) d\lambda \quad (6)$$

where

$$k_s(\lambda) = \frac{\pi d^2}{4(f\#)^2} \phi_s(\lambda) \eta(\lambda) \tau_{opt}(\lambda) \int_{z_{target}}^{z_{observe}} \tau_{atmos}(z, \lambda) dz, \quad k_b(\lambda) = \frac{\pi d^2}{4(f\#)^2} \int_{z_{target}}^{z_{observe}} (\phi_e(z, \lambda) + \phi_{sc}(z, \lambda)) \eta(\lambda) \tau_{opt}(\lambda) \tau_{atmos}(z, \lambda) dz \quad (7)$$

and other parameters are as follows: d^2 is the detector area, T is the integration time per spectral image (equal to the complete spectrum time for the fully-staring, snap-shot DIS and equal to the single-band integration time for the temporally scanned DIS), $f\#$ is the f-number of the optics, the spectral bin has a width $d\lambda$, $\phi_s(\lambda)$ is the signal radiance of the target at wavelength λ , $\eta(\lambda)$ is the quantum efficiency of the detector, $\tau_{opt}(\lambda)$ is the transmission efficiency of the imager optics, $\tau(z, \lambda)$ is the atmospheric transmission at of a thin layer of air of thickness dz at range z and wavelength λ , $z_{observe}$ is the absolute location of the imager along the line of sight, z_{target} is the absolute location of the target, and $\phi_e(z, \lambda)$ and $\phi_{sc}(z, \lambda)$ are the radiance due to atmospheric emission and scattering of a thin layer of the atmosphere. The RMS value of the detector read noise, measured in electrons is \bar{n}_d . Values for $k_s(\lambda)$ and $k_b(\lambda)$ can be readily calculated with the aid of commercial software such as *Lowtran*.

4. SNR FOR FOURIER-TRANSFORM IMAGING SPECTROMETRY

For a Fourier-transform imaging spectrometer, the calculation of the SNR are a little more complex and results in expressions at each wavenumber that are dependent on the whole spectral distribution of light transmitted to the detector. Approximate expressions are calculated here that are serviceable in all cases. The number of photoelectrons per second, $e_s(x)$, recorded at each path difference x of the interferometer used in a Fourier-transform spectrometer may be written as a bias plus the interferogram and additive noise:

$$e_s(x) = \int_0^{\infty} (k_s(\sigma) + k_b(\sigma)) T \frac{1 + \cos(2\pi\sigma x)}{2} d\sigma + n_d(x) + n_s(x) + n_b(x) \quad (8)$$

where $k_s(\sigma)$ and $k_b(\sigma)$ are defined in an analogous way to equation (7) and $k_s(\sigma) + k_b(\sigma)$ is equal to the number total of photoelectrons per second that are recorded at the grand maximum position. $n_d(x)$, $n_s(x)$ $n_b(x)$ are noise contributions at path difference x due to the detector, shot-noise on the signal and shot-noise on the background respectively. These noise components are random, non-deterministic and their values are characterized by their RMS values \bar{n}_d , $\bar{n}_s(x)$ and $\bar{n}_b(x)$ and their spectra are assumed to be white. The detector read noise, $n_d(x)$, varies randomly with path difference x , but its RMS value is independent of x . The RMS values of the shot-noise contributions are equal to the square root of the photon count of each component and so the RMS values will be modulated by a $\sqrt{(1 + \cos(2\pi\sigma x))/2}$ envelope. They are given by

$$n_{s,b}(x) = \sqrt{\int_0^{\infty} k_{s,b}(\sigma) T \frac{1 + \cos(2\pi\sigma x)}{2} d\sigma} = \sqrt{\frac{T}{2} \int_0^{\infty} k_{s,b}(\sigma) d\sigma} \sqrt{1 + I_{s,b}(x)} \quad (9)$$

where $I_{s,b}(x)$ represents the interferogram for either the target signal or the background, as appropriate. Thus the RMS values of each shot-noise component can be considered as a constant value modulated by the interferogram associated with each component and the RMS value is equal to that due to the bias multiplied by the RMS value of $\sqrt{1 + I(x)}$. In the limits of an interferogram for very broadband light or for monochromatic light the RMS value of $\sqrt{1 + I(x)}$ is equal to 1. For the continuum of bandwidths between these two extremes the RMS value of $\sqrt{1 + I(x)}$ is within a few per cent of unity. We can thus approximate

$$n_{s,b}(x) \approx \sqrt{\frac{T}{2} \int_0^{\infty} k_{s,b}(\sigma) d\sigma}.$$

(10)

We can now evaluate $k_s(\sigma)+k_b(\sigma)$ from Fourier inversion of (8). Provided that we have an estimate of $k_b(\sigma)$ we can then estimate $k_s(\sigma)$ which enables calculation of the incoming radiance $\phi(\sigma)$.

In practice, values of $e_s(x)$ are recorded at a set of discrete path differences $x_i = offset + i\delta x$ for $i = 1 \dots N_{FTIS}$ and an inverse discrete Fourier transform (DFT) is used to calculate $\phi(\sigma)$. Neglecting instrumental artifacts, the interferogram is symmetrical and only the real part of the DFT (the discrete cosine Fourier transform) is required. To emphasize that the detector read-noise is a function of only the detector electronics and not interferometry we replace $n_d(x_i)$ by $n_d(i)$ and write the inverse Fourier cosine transform of (8) as

$$\int_{\sigma}^{\sigma+\delta\sigma} (k_s(\sigma) + k_b(\sigma)) T d\sigma = \frac{2}{N_{FTIS}} \left(\sum_{i=1}^{N_{FTIS}} e_s(x_i) \cos(2\pi\sigma x_i) - \sum_{i=1}^{N_{FTIS}} n_d(i) \cos(2\pi\sigma x_i) - \sum_{i=1}^{N_{FTIS}} n_s(x_i) \cos(2\pi\sigma x_i) - \sum_{i=1}^{N_{FTIS}} n_d(x_i) \cos(2\pi\sigma x_i) \right) \quad (11)$$

If we know all of the noise vectors exactly we can calculate $k_s(\sigma)+k_b(\sigma)$ exactly and from calibration of $k_b(\sigma)$ we can calculate the required $k_s(\sigma)$. However the noise components are random processes that limit the accuracy with which we can calculate $k_s(\sigma)+k_b(\sigma)$. We therefore make an estimate $\tilde{k}_s(\sigma) = k_s(\sigma) + k_b(\sigma) - \tilde{k}_b(\sigma) + n(\sigma)$ where $\tilde{k}_b(\sigma)$ is an estimate of the background signal and $n(\sigma)$ is the noise component. The SNR is therefore given by the ratio of the signal to the noise component: $k(\sigma)/n(\sigma) \approx \tilde{k}(\sigma)/n(\sigma)$. We now estimate this value.

The signal-to-noise ratio for the calculation of $k(\sigma)$ is equal to the SNR for $\phi(\sigma)$ and is given by the ratio of the first component in equation (11) to the quadrature sum of the three noise components. The sum of each noise component at each spatial frequency is essentially the sum of a sequence of random numbers multiplied by a cosine weighting function. This expectation of the RMS value of this sum is equal to the product of the RMS value of the noise, the RMS value of the weighting function ($1/\sqrt{2}$) and the square root of the number of samples. The SNR may then be written directly as

$$SNR(\sigma) = \frac{T_{tot} \int_{\sigma}^{\sigma+\delta\sigma} k_s(\sigma) d\sigma}{\sqrt{2N_{FTIS} \bar{n}_d^2 + T_{tot} \int_{\sigma_{min}}^{\sigma_{max}} k_s(\sigma) d\sigma + T_{tot} \int_{\sigma_{min}}^{\sigma_{max}} k_b(\sigma) d\sigma}} \quad (12)$$

where $T_{tot} = N_{FTIS} T$ is the total integration time during the scanning of the Fourier-transform spectral imager. Due to time lost stepping the path difference and reading out the detector, the total integration time will normally be shorter time than the total time required to record the spectral image.

There are several important differences between equation (12) and the expression for the SNR of a DIS (equations(5)-(7)):

- For a Fourier-transform spectrometer the shot-noise contribution is due to the full spectral band $\Delta\sigma = \sigma_{max} - \sigma_{min}$ rather than a single spectral bin (note the limits in the integrals: $\sigma_{max}, \sigma_{min}$ in equation (12) compared to $\lambda, \lambda + \delta\lambda$ in (6).)
- The total noise contribution from the detector reads is a factor of N_{FTIS} greater (the factor of two in equation (12) is due to the factor described next)
- The average optical transmission, for a conventional Fourier-transform instrument, is limited to 50%.
- The total integration time $T_{tot} = N_{FTIS} T$, is the total spectrum time (rather than the time taken to record the image in a single spectral band). This increase in optical throughput is the Fellgett multiplex advantage.

Equation (12) can also be used for the SNR of a FS-FTIS provided an appropriate definition of is used; that is, for the FS-FTIS, T is both the total integration time and the phase step time ($T_{tot} = T$). The justification is as follows. Equations (8) to (12) may be employed as above with the exception that the radiance at the instrument aperture is amplitude divided onto N_{FTIS} detectors by the anamorphic input optics in the FS-FTIS. The reduction in irradiance at each detector is compensated by the increased integration time (assuming no pushbroom scanning of the slit across the scene) which can be N_{FTIS} times longer. Thus if the total integration times $T_{tot} = N_{FTIS} T$ of the temporal FTIS and $T_{tot} = T$ for the spatial FTIS are equal, the N_{FTIS} factor cancels and the SNR in both cases is equal and is given by equation (12). That is, the SNR in the two-dimensional

spectral image of the FTIS recorded in time T_{tot} is equal to the SNR in a single line image produced by a FS-FTIS that has stared at the same single line in the scene for the same integration time T_{tot} . Of course the spectral images produced by the two techniques are not directly comparable, since the temporally scanned FTIS enables the recording of a two-dimensional spectral image during the total integration time whereas the spatial FTIS records a spectral image of only a single line and will generally need to be scanned to form a two-dimensional image. If the slit of the spatial FTS is scanned across N_y pixels, the total integration time will be a factor of N_y shorter with a consequent reduction of the SNR. This is the usual spatial multiplex disadvantage associated with pushbroom scanning a slit image across the scene.

5. COMPARISON OF SIGNAL-TO-NOISE RATIOS OF DIRECT AND FOURIER-TRANSFORM IMAGING SPECTROMETERS

Direct imaging spectrometry and Fourier-transform imaging spectrometry produce record speclal data cubes through fundamentally different processes and an exact comparison between equivalent systems is not possible. For example:

- The SNR in each spectral bin of a DIS is independent of the signals occurring in all other spectral bins, whereas for a FTIS it is not.
- One read of a detector is required for the DIS for each spectral bin, whereas for a FTIS, sampling of a double-sided interferogram at more than twice the highest spatial frequency in the interferogram requires at least a factor of two more detector reads. The FTIS returns measurements of all spectral wavenumber down to zero frequency, although in practice there is no information of interest below the low frequency cut-off of the detection system. For the 8-12 μm band, double-sided sampling of the interferogram at twice the highest spatial frequency in the interferogram (that is Nyquist sampling) results in six times greater detector reads than an equivalent DIS. However, it is possible, in principle, to reconstruct the spectrum by sampling only one side of the interferogram and by sampling at the Nyquist spatial frequency for the bandwidth of spatial frequencies in the interferogram, rather than for the highest spatial frequency. In this case the number of detector reads is equal for both the DIS and FTIS. The number of detector reads per spectrum is a particularly important parameters since a high number may result in a requirement for an excessive detector frame rate.
- The spectral resolution for a DIS tends to be constant in the wavelength domain, whereas the spectral resolution of the FTIS is constant in the wavenumber domain.
- Random access to spectral bands is possible with a DIS, whereas for a FTIS all contiguous spectral bins are reconstructed simultaneously and random access is possible.

Fortunately the same mathematical formulation can be used both for a DIS and for a FS-DIS that is spatially scanned across the scene. In fact, if the degree of spectral multiplexing is equal to the degree of spatial multiplexing then the SNRs are equal and the data rate, in terms of voxels (a pixel element with co-ordinates (x,y,λ)) in the data cube per time interval will also be equal. We may treat these together by employing the single parameter N_{MPX} which we use to represent either the spatial or spectral multiplex factor used to construct the data cube.

For purposes of analysis, we can thus choose the shape of the spectral cube to be whatever is most convenient for comparison of SNRs. For comparison of one-dimensional snapshot imaging spectrometers, such as pushbroom scanned FS-DIS and FS-FTIS systems, we set $N_{MPX}=1$. If we wish to compare the SNRs of a two-dimensional spectrally multiplexed imager with a two-dimensional FTIS then $N=N_{MPX}$ is equal to the number of contiguous spectral channels into which the spectrum of interest is channelised.

We now derive the equations that enable comparison of the SNRs of the direct and Fourier-transform techniques for equal volumes of data cube, that is for equal numbers of voxels. This enables (a) the comparison of FTIS with DIS and (b) one-dimensional FS-DIS and FS-FTIS instruments. Using equations (6) and (12), the ratio of the SNR of a DIS to the SNR of a FTIS can be written as

$$\frac{SNR_{FTIS}(\sigma)}{SNR_{DIS}(\sigma = 1/\lambda)} = \sqrt{\frac{N_{MPX} T_{tot}^{FTIS} \int_{\sigma}^{\sigma+\delta\sigma} k_s(\sigma) d\sigma}{T_{tot}^{DIS} \int_{\lambda}^{\lambda+\delta\lambda} k_s(\lambda) d\lambda}} \sqrt{\frac{\frac{N_{MPX} \bar{n}_d^2}{T_{tot}^{DIS}} + \int_{\lambda}^{\lambda+\delta\lambda} k_s(\lambda) d\lambda + \int_{\lambda}^{\lambda+\delta\lambda} k_b(\lambda) d\lambda}{\frac{2N_{FTIS} \bar{n}_d^2}{T_{tot}^{FTIS}} + \int_{\sigma_{min}}^{\sigma_{max}} k_s(\sigma) d\sigma + \int_{\sigma_{min}}^{\sigma_{max}} k_b(\sigma) d\sigma}}$$

(13)

We assume that the spectral transmissions $\tau^{FTIS}(\sigma)$ and $\tau^{DIS}(\lambda)$ do not vary strongly with wavelength and can be replaced by nominal values τ^{FTIS} and τ^{DIS} . To enable us to write easily interpretable expressions we assume that the input spectra are gray so that $k_s(\sigma)$ and $k_b(\sigma)$ are constant with respect to σ and hence at this level of approximation, so are $k_s(\lambda)$ and $k_b(\lambda)$ (it should be noted that it is mathematically inconsistent for both $k(\lambda)$ and $k(\sigma)$ to be simultaneously gray, but this is a useful approximation). Bearing this caveat in mind, we can write that since the total incident flux is identical in both cases we can write

$$N \frac{\int_{\sigma}^{\sigma+\delta\sigma} k_s(\sigma) d\sigma}{\tau^{FTIS}} = N \frac{\int_{\lambda}^{\lambda+\delta\lambda} k_s(\lambda) d\lambda}{\tau^{DIS}}. \quad (14)$$

where N is the total number of spectral bands. In equation (13) T_{tot}^{FTIS} and T_{tot}^{dir} are the total integration times used by the detectors in the FTIS and DIS to record a spectral image cube. For equal radiance at the entrance apertures of the two instruments, the total irradiance at the detector of the FTIS is greater than for the DIS, due to the need to simultaneously record input flux across the full spectral bandwidth σ_{min} to σ_{max} rather than across only a single spectral bin λ to $\lambda+\delta\lambda$. One consequence is that for high radiance levels it is necessary to reduce the detector integration time T_{tot}^{FTIS}/N_{FTIS} to prevent detector saturation and this limits the SNR of the FTIS.

We use the following constants to describe the input photon flux

$$K_s = \frac{\int_{\lambda}^{\lambda+\delta\lambda} k_s(\lambda) d\lambda}{\tau^{DIS}} = \frac{1}{N_{spect}} \frac{\int_{\sigma_{min}}^{\sigma_{max}} k_s(\sigma) d\sigma}{\tau^{FTIS}} \quad K_b = \frac{\int_{\lambda}^{\lambda+\delta\lambda} k_b(\lambda) d\lambda}{\tau^{DIS}} = \frac{1}{N_{spect}} \frac{\int_{\sigma_{min}}^{\sigma_{max}} k_b(\sigma) d\sigma}{\tau^{FTIS}} \quad (15)$$

which can be inserted into equation (13) to give

$$\frac{SNR_{FTIS}}{SNR_{DIS}} = \frac{\tau^{FTIS}}{\tau^{DIS}} \sqrt{\frac{N_{MPX} T_{tot}^{FTIS}}{T_{tot}^{DIS}}} \sqrt{\frac{N_{MPX} \frac{\bar{T}}{T_{tot}^{DIS}} + \frac{\tau^{DIS}}{N_{spect}}}{2N_{FTIS} \frac{\bar{T}}{T_{tot}^{FTIS}} + \tau^{FTIS}}} \quad (16)$$

where the following identities have been applied:

$$\bar{T} = \frac{\bar{n}_d^2}{N_{spect} K_s (1 + \beta)} \quad \beta = \frac{K_b}{K_s} \quad \gamma = \frac{N_{FTIS}}{N} \quad (17)$$

We make the following comments about these parameters. \bar{T}/τ^{FTIS} is the time taken for the output of the detector to give a signal-to-noise ratio of unity at the grand maximum of the FTIS interferogram. \bar{T} is therefore dependent only on the detector read noise and the scene imaged by the detector. It is small for high radiance and for low detector noise. β is the ratio of background radiance to target radiance. It will be small for short-range imaging and large for long-range imaging through an optically thick atmosphere. γ is the ratio of FTIS phase steps to spectral bins. This will be equal to unity for Nyquist sampling of the interferogram spatial frequency bandwidth and may be as large as six or more for Nyquist sampling of the highest spatial frequency in the interferogram.

The parameter \bar{T} is related to the integration time per detector read required to achieve shot-noise limited spectral imaging and this is a factor of $N/2$ longer for the DIS. This is illustrated in Figure 1 where we plot the ratio given by equation (16) as a function of T_{tot}/\bar{T} where T_{tot} is the total integration time taken to record the spectrum. We see that for small values of T_{tot}/\bar{T} to the left of both dotted lines, both FTIS and DIS SNRs are detector-noise limited, the SNR of the FTIS is greater than the SNR of the DIS and this advantage increases with increasing N . In the area between the dashed lines, the FTIS is shot-noise limited, but the DIS is detector-noise limited and the FTIS still offers a SNR advantage. At high values of T_{tot}/\bar{T} and small numbers of spectral bins, both the DIS and FTIS SNRs are shot-noise limited and the ratio asymptotically approaches unity. This analysis assumes that no detector saturation occurs.

As T_{tot} / \bar{T} increases, both SNR_{FTIS} and SNR_{DIS} increase up to the point at which the number of photoelectrons stored at the detector pixel is equal to the detector well capacity and for higher levels of irradiance at the detector no further increase in the SNRs is possible. Due to the high detector irradiances that occur in an FTIS, the FTIS detector saturates at a lower value of T_{tot} / \bar{T} than the DIS. Thus if we now replot Figure 1 taking into account detector saturation, we find that as T_{tot} / \bar{T} increases, the ratio SNR_{FTIS} / SNR_{DIS} remains approximately level until the point at which the detector in the FTIS saturates. Further increases in T_{tot} / \bar{T} reduces SNR_{FTIS} / SNR_{DIS} until the value of T_{tot} / \bar{T} at which the DIS also saturates above which the SNR is constant. This is shown in Figure 2 for (a) a 3-5 μm detector with a 20 million electrons well capacity and (b) for a 8-12 μm detector with a 70 million electron well capacity.

To apply the data plotted in Figure 2 it is necessary to know the value of T_{tot} / \bar{T} for a specific application. This is governed mainly by the system etendue, the scene and background irradiance, and the camera frame rate. Typical values and related parameters for each of the spectral bands are shown in Table 2 for imaging at nadir from a height of 1,500 m. Values for K_s and K_b were calculated with *Lowtran 7* and salient parameters are indicated in the caption. From the data presented it can be seen that the FTIS offers a SNR advantage for low flux and large numbers of spectral bands. For a given number of spectral bands, the SNR advantage of the FTIS can be seen to be greatest in the 3-5 μm band where values of T_{tot} / \bar{T} are low and the relatively large detectors result in large well capacities. In the 8-12 μm band typical values of T_{tot} / \bar{T} are almost two orders of magnitude higher so that only for large numbers of spectral bands does the FTIS offer a SNR advantage. The minimum number of spectral bands at which the FTIS offers superior SNR to the DIS is summarized in Table 3 for typical parameters and camera rates of 800 Hz and 40 Hz. For imaging through a gray atmosphere the ratio $\beta = K_b / K_s$ is non-zero and it can be seen from equation (17) that the data shown in Figure 2 can be used by calculating K_s and multiplying the abscissa by $(1+\beta)$.

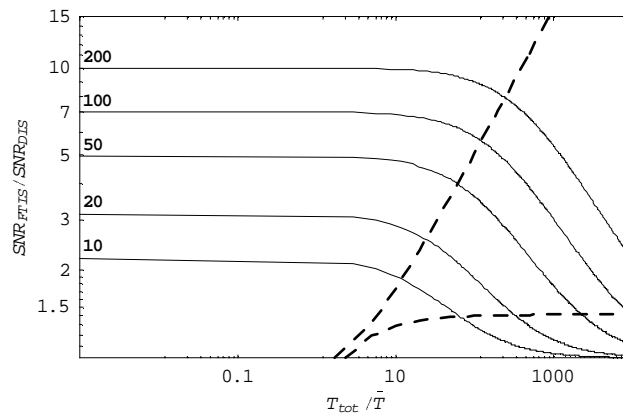


Figure 1 Depiction of the regions of detector-noise and shot-noise limited operation of the FTIS and the DIS when $\gamma=1$. See text for a further explanation.

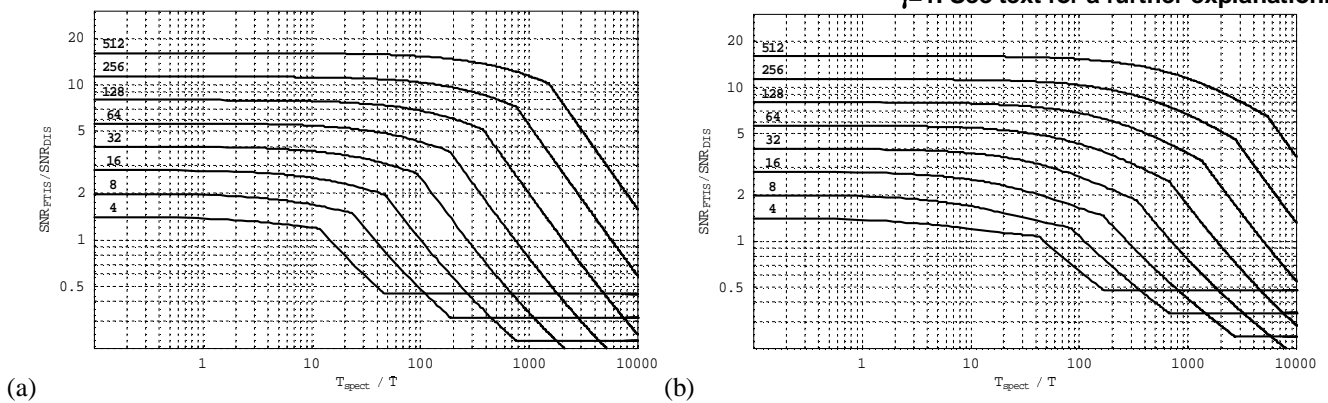


Figure 2 Variation of ratio of FTIS and DIS signal-to-noise ratios with normalised detector signal T_{tot} / \bar{T} for the indicated numbers of spectral bins

Waveband	Range	NK_s (ph/s)	NK_b (ph/s)	\bar{T} (msec)	N	T_{int}/\bar{T} at camera rate		T_{tot}/\bar{T} at camera rate	
						800 Hz	40 Hz	800 Hz	40 Hz
Visible	Zero	5.1×10^8	0	0.078	20	16	317	317	6342
	1500m	2.4×10^8	1.4×10^9	0.025		50	1008	1009	20174
NIR	Zero	2.3×10^8	0	0.11	20	12	232	232	4646
	1500m	1.5×10^9	4.6×10^9	0.041		31	616	616	12321
MWIR	Zero	2.6×10^8	0	2.6	10	0.47	9.5	4.7	95
	1500m	1.4×10^9	2.4×10^9	1.8		0.69	14	6.9	138
LWIR	Zero	6.8×10^{11}	0	0.0099	10	126	2520	1260	25208
	1500m	4.8×10^{11}	4.0×10^{11}	0.0076		164	3290	1645	32908

Table 2 Table of typical values for K_s , K_b , \bar{T} and T_{int}/\bar{T} for imaging at zero range and at Nadir for a 1500m vertical path in each of the atmospheric windows for f/2 systems using typical parameters for detector arrays and for a target with albedo of 0.2 in temperate solar illumination at noon. \bar{T} is approximately equal to the time required such that the photon shot-noise on the output of a conventional fully staring detector (without spectral filters) is equal to detector noise.

Waveband	N (800 Hz)	N (40 Hz)
Visible	65	489
NIR	173	1283
MWIR	1	15
LWIR	49	394

Table 3 Values of N above which the FTIS enables higher SNRs than DIS in each waveband at 800 Hz and 40 Hz camera rates.

6. COMPARISON OF SIGNAL-TO-NOISE RATIOS OF ONE-DIMENSIONAL FS-DIS AND FS-FTIS

In this section we use (16) to make the very pertinent comparison between the SNRs of a push-broom scanned, one-dimensional FS-DIS and a push-broom scanned, one-dimensional FS-FTIS. In both cases an image of the input slit is dispersed across a two-dimensional detector. For a FS-DIS, the dispersion is according to wavelength. For the FS-FTIS, the dispersion is according to path difference between interfering components. Both systems propagate all light incident at the slit to the detector arrays, so the FTIS exhibits no Fellgett multiplex advantage over the DIS. However, for the FTIS, shot-noise on the bias couples into all spectral bins causing an increased noise floor as can be appreciated from equation (12). As a consequence, we would expect the SNR of a one-dimensional imaging spatial Fourier-transform spectrometer to be generally poorer for broadband light than a one-dimensional dispersive direct imager. This is not necessarily true for non-imaging Fourier-transform instruments for which the Jacquinot etendue advantage means that the Fourier-transform instrument can have a higher optical throughput¹².

To deduce the ratio of SNRs, we use equation (16), setting $N_{MPX}=1$, since in both cases there is no multiplexing of the input signal and setting equal total integration time in each case we can write the ratio of the SNRs in the shot-noise and detector-noise limits as

$$\left. \frac{SNR_{FS-FTIS}}{SNR_{FS-DIS}} \right|_{\text{Shot-noise limit}} = \sqrt{\frac{\tau^{FTIS}}{\tau^{DIS} N_{spect}}} \quad \left. \frac{SNR_{FS-FTIS}}{SNR_{FS-DIS}} \right|_{\text{Detector-noise limit}} = \frac{\tau^{FTIS}}{\tau^{DIS}} \sqrt{\frac{1}{2N_{FTIS}}} \quad (18)$$

So we see that assuming the optical transmission efficiencies are similar, the SNR of the spatial FTS will be worse than the equivalent dispersive imaging spectrometer in all cases except for imaging of monochromatic light, for which the shot-noise limited SNRs are equal. We conclude that the SNR of the FS-DIS will normally be superior to the SNR of the FS-FTIS.

It is straightforward to use the equations presented in this paper to calculate the ratios of the SNRs involving a FS-DIS, such as a fiber-coupled device by setting $N_{MPX}=1$. This enables equation (16) to be used to calculate the ratio SNR_{FS-DIS}/SNR_{FTIS} and equation (5) and (15) to be combined to calculate the ratio SNR_{FS-DIS}/SNR_{DIS} . One then finds that in the former case SNR_{FS-DIS}/SNR_{FTIS} varies between about \sqrt{N} and $\sqrt{\lambda N}$ between the shot-noise and detector-noise limited conditions and detector saturation has little impact on these values. In the latter case, SNR_{FS-DIS}/SNR_{DIS} varies between $\sqrt{N_{MPX}}$ in the shot-noise limit and N_{MPX} in the detector-noise limit. Detector saturation however limits the SNR advantage of FS-DIS over DIS in all wavebands to high values of N and relatively high detector frame rates.

7. CO-REGISTRATION

Wide field of view imaging spectrometry in more than a handful of spectral bands requires some form of temporal multiplexing or scanning, as with a spectrally multiplexed DIS or a temporally scanned FTIS. This scanning introduces the problem of coregistration of sub-images illustrated in Figure 3(a). As the target tracks through the ground footprint, the intensity of the image on the detector varies according to the convolution of the target intensity distribution with the footprint of the imaging optics and this will vary between spectral sub-images or interferometer phase steps. Misregistration between consecutive sub-images leads to differing relative intensities in each spectral band or phase step and this leads to distortion of spectra that cannot be calibrated post-detection. Distortion of the spectra can be ignored provided that the relative motion between the scene and the imager is kept small; below the noise floor of the imager for example. The graph in Figure 3(b) shows the fractional variation in responsivity as a uniformly colored square target is tracked across the center of an imager footprint that is approximated by an Airy disk and when the target sides are of dimensions 0.0001, 0.5, 1 and 2 pixels. Clearly the problem is most severe when the square (or feature sizes) are small and from the figure we can estimate that for fractional errors of less than 0.01 and 0.001 (for SNRs of 100 and 1,000), misregistration must be less than about 1/20 and 1/50 of a pixel respectively, but this requirement can be significantly relaxed for target dimensions bigger than about one pixel.

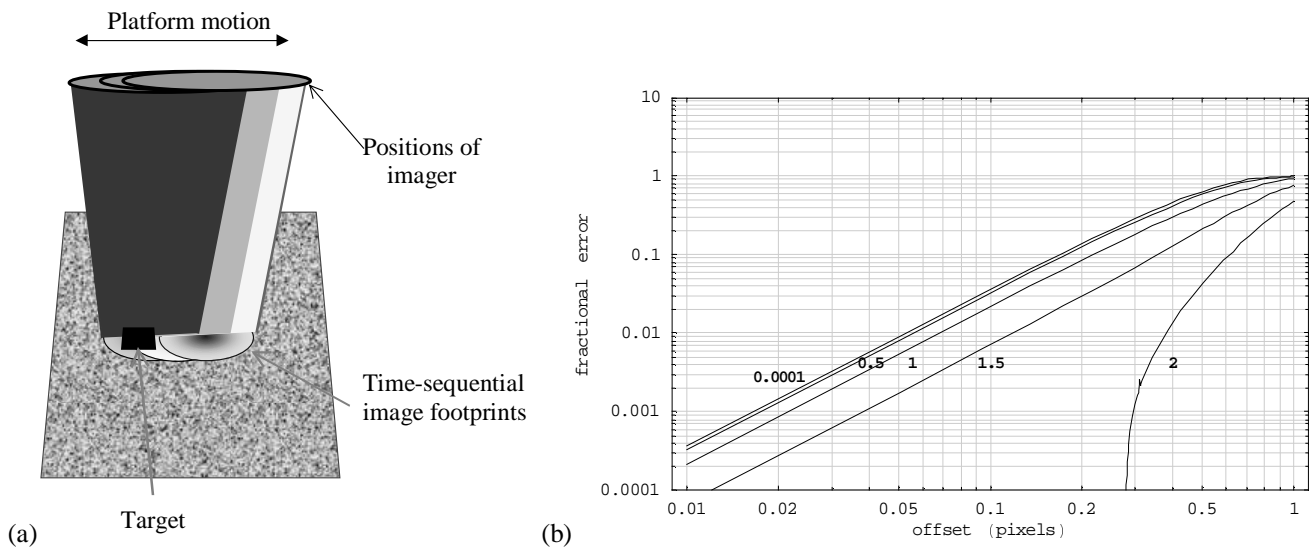


Figure 3 (a) Illustrates the distortion in spectra introduced by relative motion between an imaging spectrometer and the scene and (b) shows how the resultant fractional error varies with misregistration offset for several sizes of target (both measured in pixels)

8. MODELLING OF SIGNAL-TO-NOISE RATIOS

In the previous sections we have discussed the required SNR and coregistration for spectral imaging and the relative SNRs that the four generic classes of imaging spectrometer offer. To enable simple equations to be written a gray spectrum was assumed and some mathematical simplifications were made so that equations could be written that are not rigorously accurate are general and easily interpreted. In this section we illustrate these points numerically without the need to resort to mathematically inconsistent simplifications. We use the example of wide field surveillance from a slow flying aircraft flying at an altitude of 1,500 m. For these parameters a point on the ground passes through the footprint of a single pixel in about 1/40 of a second. If we require a SNR of about 100, we can see from Figure 3(b) that coregistration of better than 1/20 of a pixel is required, suggesting that if no tracking is used the camera frame rate would need to be $800N$, where N is greater than 10. Such high frame rates of greater than 8 kHz are considered impractical, so we assume here that a track and stare technique is employed to stabilize the image on the detector during the acquisition time for a single spectral image cube. The rate at which the spectral image cube is generated is then determined by the required update rate and the maximum duration for which the scene can be stabilized. We therefore assume a spectral data cube rate of 40 Hz.

Values of $k_s(\lambda)$, $k_b(\lambda)$, $k_s(\sigma)$, $k_b(\sigma)$ were calculated using *Lowtran 7* and the calculated SNRs are plotted in Figure 4 for the medium-wave (MWIR) and long-wave (LWIR) infrared bands. It is assumed that the spectrum is sampled in ten spectral bands by each technique except for the partial DIS which records a selection of only five out of ten bands (and hence enables twice the integration time per spectral band). In calculating this data it was assumed that for the partial DIS and FS-DIS techniques the camera frame rate would be adjusted between a minimum of the spectrum refresh rate of 40 Hz and the

maximum detector rate of 400 Hz. That is it is the minimum rate that simultaneously avoids saturation and enables the required data cube rate. This enables the frame rate to be increased for these techniques and frame-to-frame integration to be used so that the impact of detector saturation can be limited and the total integration time can be maximized. This has resulted in the very high predicted SNRs for the FS-DIS techniques. The wide field-of-view FS-DIS with high angular resolution and modest-to-high spectral resolution is, to some extent, a theoretical construct that is useful only as a reference point (although it could be in principle be implemented using, for example, arrays of optical fiber coupled spectrometers). The SNRs for the FS-DIS predicted here are equal to those for a classical pushbroom scanned one-dimensional DIS, although this is not normally considered as a real-time image since it is one-dimensional. Similar data are shown in Figure 4 (c) and (d) for imaging in 100 bands (20 bands for the partial DIS), but it is assumed that a maximum detector rate of 1 kHz limits the spectrum frame rate to 10 Hz.

It can be seen that, for imaging in the photon-starved MWIR band with low spectral resolution, all techniques offer similar SNRs, within a factor of two, but at high spectral resolutions the FTIS offers SNRs that are over ten-fold higher. The SNRs of the partial DIS are similar to the FTIS although this will only be relevant if similar discrimination can be achieved from the reduced number of spectral bands in the partial DIS. In the LWIR band the high photon irradiances cause rapid detector saturation that severely limits the attainable integration times for the FTIS and FS-DIS. Detector well-capacity is thus a major factor in determining the achievable SNRs in the LWIR. It should be noted that these calculated SNRs are based on somewhat ideal models and the actual SNRs, particularly in the MWIR, may be up to a factor of two lower than those calculated.

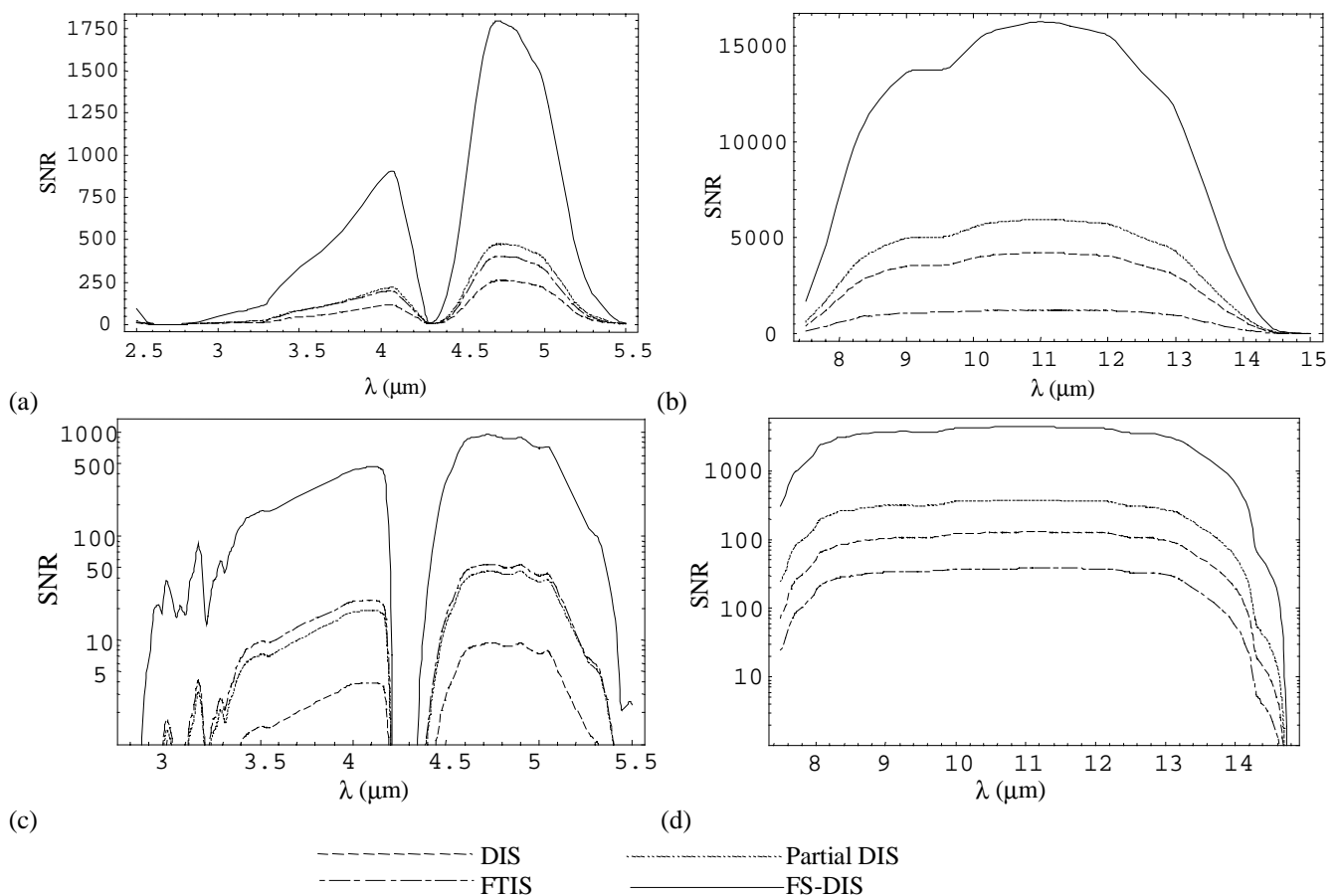


Figure 4 (a) and (b) Calculated variation in SNRs in the medium wave and long wave infrared bands for imaging spectrometry of the ground at nadir from a slow flying aircraft. The four techniques modelled are ten-waveband imaging using DIS, FS-DIS and FTIS and for partial DIS using 5 of these bands. The detector rate is the minimum that is necessary to prevent saturation and is in the range 40-400 Hz. Frame-to-frame signal averaging enables higher SNRs to be obtained with the partial DIS and FS-DIS techniques. SNR curves are shown in (c) and (d) for imaging in 100 bands (20 bands for partial DIS) at 10 Hz spectrum rate.

As stated in section 2, whether the calculated SNRs are high enough to be useful depends very much on the similarity of the spectra that must be distinguished. However for typical tasks of spectrum discrimination one can conclude that the SNRs shown in Figure 4 (a), (b) and (d) are probably adequate. The SNRs shown in Figure 4 for high resolution spectral imaging in the MWIR band are probably lower than might be desired and improved spectral discrimination may be obtainable from the improved SNR that will be obtained from reduced spectral resolution (provided that the spectra to be discriminated are slowly varying).

CONCLUSIONS

The principles for defining, comparing and calculating the signal-to-noise ratio performance of imaging spectrometers have been presented with an emphasis on real-time applications. The technique that offers the highest SNRs depends on factors such as the waveband for application and required spectral resolution. For high spectral resolution and the low irradiances that occur in, for example, the 3-5 μm band, SNRs are detector-noise limited and the Fourier-transform imaging spectrometer is predicted to offer the higher signal-to-noise ratios. In the 8-14 μm band detector photon radiance is much higher and SNRs are shot-noise limited and furthermore tend to be determined by detector saturation levels. This latter point discriminates against Fourier-transform methods and so in the LWIR and for applications with high detector irradiances in general, SNRs are higher for the DIS techniques. However, the use of these temporally scanned techniques for real-time imaging spectrometry, such as is required for wide-field of view airborne surveillance, is only feasible if good spectral coregistration can be achieved otherwise a snapshot imaging technique must be used. Interestingly, it is shown here that in all circumstances the spatial Fourier-transform snapshot imaging spectrometer offers inferior SNRs to the direct snapshot imagers. Implementation of a wide field of view, snapshot imaging spectrometer with reasonable spectral resolution is problematic, but since such a device would require no step stare stabilization and SNRs are significantly higher, developments in this area would be welcome.

ACKNOWLEDGEMENT

This work was funded under extra mural research contracts from DERA, Malvern, UK

REFERENCES

- ¹ J Oleson, R Jungquist and Z Ninkov, "Tuneable multispectral imaging system technology for airborne applications" SPIE 2480, Aerosense '95, Imaging spectrometry pp 280-285 (1995)
- ² J C Demro, R Hartsorne, L M Woody, P A Levine, J R Tower, "Design of a multispectral wedge-filter remote-sensing instrument incorporating a multi-port, thinned CCD area array", SPIE 2480, Aerosense '95, Imaging spectrometry pp 280-285 (1995)
- ³ P Mouroulis, 'Spectral and spatial uniformity in push-broom imaging spectrometers', Imaging spectrometry V, SPIE 3753 pp 133-141 (1999)
- ⁴ G R O Vane, T G Green, H T Chrien, E G Hanson, W M Porter, 'The airborne visible/infrared imaging spectrometer (AVRIS)' Remote Sen. Environ., **44**, pp127-143, (1993)
- ⁵ T Wilson, C Davis, 'Naval EarthMap Observer (NEMO) Satellite', Imaging Spectrometry V, SPIE 3753, pp 2-11 (1999)
- ⁶ J A Hackwell et al, "LWIR/MWIR imaging hyperspectral sensor for airborne and ground-based remote sensing", Proc. SPIE **2819**, pp 274-283 (1995)
- ⁷ R W Basedow, D C Carmer, M L Anderson, 'HYDICE system implementation and performance' SPIE 2480, pp 258-267 (1995)
- ⁸ A. Peacock, P Verhoeve, N Rando, A van Dordrecht, B G Taylor, C Erd, M A C Perryman, R Venn, J Howlett, D J Goldie, J Lumley, M Wallis, 'Single optical photon detection with a superconducting tunnel junction', Nature, **381**, pp 135-136, (1996)
- ⁹ C L Bennett, M R Carter, D J Fields, 'Hyperspectral imaging in the infrared using LIFTIRS', Proc. SPIE **2552**, pp 274-283, (1995)
- ¹⁰ W Wadsworth, J P Dybwad, 'Ultra-high speed chemical imaging spectrometer', Proc. SPIE **3082** pp 148-154, (1997)
- ¹¹ A D Meigs, E W Butler, B A Jones, L J Otten III, 'Airborne visible hyperspectral imaging spectrometer:optical and system level description', SPIE **2819**, pp 278-284, (1996)
- ¹² A R Harvey, 'Determination of the optical constants of thin film in the visible by static dispersive Fourier-transform spectrometry', Rev. Sci. Instr. (1998)
- ¹³ M R Descour, C E Volin, E L Dereniak, K J Thome, A B Schumaker, D W Wilson, P D Maker, 'Demonstration of a high speed non-scanning imaging spectrometer', Optics letters, **22**, 16, pp 1271-1273 (1997)
- ¹⁴ D M Lyons, K Whitcomb, 'Characterisation of the DOIS prototype: a diffractive optic image spectrometer', SPIE **2819**, pp 206-217 (1996)
- ¹⁵ R F Horton, "High etendue imaging Fourier-transform spectrometer", US patent 5777736, July 19 1996
- ¹⁶ Aster data base, web address <http://asterweb.jpl.gov/>